Green's function as a defect state in a boundary value problem

Jose D. H. Rivero● and Li Ge

College of Staten Island, CUNY, Staten Island, New York 10314, USA
and The Graduate Center, CUNY, New York, New York 10016, USA

A perspective of the Green's function in a boundary value problem as the only eigenstate in an auxiliary formulation is introduced. In this treatment, the Green's function can be perceived as a defect state in the presence of a δ-function potential, the height of which depends on the Green's function itself. This approach is illustrated in one-dimensional and two-dimensional Helmholtz equation problems, with an emphasis on systems that are open and have a non-Hermitian potential. We then draw an analogy between the Green's function obtained this way and a chiral edge state circumventing a defect in a topological lattice, which shines light on the local minimum of the Green's function at the source position.

I. INTRODUCTION

The Green's function is an effective tool to solve linear differential equations [1,2], both theoretically and numerically. More importantly, it provides a fundamental connection between the source and its field [3], as already recognized in its original form in the three-dimensional Laplace equation [4] and preceding Dirac's introduction of the δ function by more than a century. When extended to address dynamical equations and their spectral representations, the Green's function becomes the propagator that is essential to field theories [5]. As such, the Green's function is a powerful and indispensable utility in a variety of transport and scattering problems, ranging from condensed-matter physics [6,7], optics and photonics [8–10], to high-energy physics [11].

In this article we introduce a difference perspective of the Green's function, i.e., treating it as the single eigenstate in an auxiliary boundary value problem. In addition to further enrichment and shaping of our physical intuition through the Green's function, we find exceptional parallels between the Green's function and defect states due to a local potential, including a chiral edge state circumventing a defect on its path in a topological lattice.

Below we introduce formally the Green's function problem and lay out the fundamentals of our approach. The Green's function of an operator $\mathcal{L}$ in a variety of physics problems can be defined by

$$[z - \mathcal{L}(\boldsymbol{r})]G(\boldsymbol{r}, \boldsymbol{r}'; z) = \delta(\boldsymbol{r} - \boldsymbol{r}'), \tag{1}$$

with a proper boundary condition. Here z is a parameter (e.g., the energy) and $\boldsymbol{r}, \boldsymbol{r}'$ are the coordinates of the field and the source, respectively. A different perspective of the Green's function can be obtained using the following auxiliary eigenvalue problem:

$$[z - \mathcal{L}(\boldsymbol{r})]\psi_m(\boldsymbol{r}, \boldsymbol{r}') = \lambda_m(\boldsymbol{r}')V(\boldsymbol{r}, \boldsymbol{r}')\psi_m(\boldsymbol{r}, \boldsymbol{r}'). \tag{2}$$

As we will show, this auxiliary problem has a *single* eigenvalue $\lambda_0(\boldsymbol{r}')$ and eigenstate $\psi_0(\boldsymbol{r}, \boldsymbol{r}')$ for a given source

position $\boldsymbol{r}'$, *when* $V(\boldsymbol{r}, \boldsymbol{r}')$ is chosen to be $\delta(\boldsymbol{r} - \boldsymbol{r}')$. The Green's function is then uniquely determined by

$$G(\boldsymbol{r}, \boldsymbol{r}') = \frac{\psi_0(\boldsymbol{r}, \boldsymbol{r}')}{\lambda_0 \psi_0(\boldsymbol{r}', \boldsymbol{r}')}, \tag{3}$$

and λ_0^{-1} gives the value of the Green's function at the source $\boldsymbol{r} = \boldsymbol{r}'$. As a bonus, we obtain directly the local density of states (LDOS) that is proportional to the imaginary part of $G(\boldsymbol{r}, \boldsymbol{r}; z)$ [7], i.e., $\text{Im}[\lambda_0^{-1}]$. The reciprocity of the Green's function, though implicit in Eq. (3), can be easily verified in the absence of an effective magnetic field, as shown in Appendix A. Note that we have suppressed the $\boldsymbol{r}'$ dependence of λ_0 in Eq. (3) for conciseness. Below we will do the same for the $\boldsymbol{r}$ dependence of $\mathcal{L}$ and the dependence of ψ_m on its second argument, i.e., the position of the source.

Before we apply this approach to various Hermitian and non-Hermitian problems, we first prove Eq. (3) and discuss the general properties of $\psi_m(\boldsymbol{r})$. With the choice of $V(\boldsymbol{r}, \boldsymbol{r}')$ mentioned above, the right-hand side of Eq. (2) for $\psi_0(\boldsymbol{r})$ is simply

$$\lambda_0 \delta(\boldsymbol{r} - \boldsymbol{r}')\psi_0(\boldsymbol{r}) = \lambda_0 \delta(\boldsymbol{r} - \boldsymbol{r}')\psi_0(\boldsymbol{r}'), \tag{4}$$

from which Eq. (3) follows directly by comparing with Eq. (1), with the requirement $\psi_0(\boldsymbol{r}') \neq 0$. If there were another eigenstate $\psi_{m \neq 0}(\boldsymbol{r})$, then by repeating the same procedure we would find that the Green's function is proportional to $\psi_{m \neq 0}(\boldsymbol{r})$ as well, which contradicts the uniqueness of the Green's function with a properly imposed boundary condition. When implemented numerically, there do exist spurious eigenvectors $\psi_{m \neq 0}(\boldsymbol{r})$, which, however, can be easily discarded due to their ill-behaved λ_m's, as we will discuss in Sec. II A.

The auxiliary eigenvalue approach equips us with a conceptually different way to treat the Green's function, i.e., as a defect state [12] emerging due to the δ-function potential:

$$[\mathcal{L} + \lambda_0 \delta(\boldsymbol{r} - \boldsymbol{r}')]\psi_0(x) = z\psi_0(x). \tag{5}$$

As we will show, this point of view is particularly interesting and helpful in a topological system with chiral edge states [13–17]. For example, if a point source is placed at the edge of a two-dimensional (2D) topological insulator, the auxiliary eigenvalue approach indicates that an analogy exists between the Green's function and a chiral edge state circumventing a defect at the same location. This interpretation provides an intuitive understanding of the local minimum of the Green's function at the source position, which we will illustrate using a 2D square lattice with a $\pi/2$ Landau gauge.

The rest of the paper is organized into two main parts, where we validate our method and discuss the insight it provides, respectively. In Sec. II, we first validate our method in a one-dimensional (1D) Hermitian (closed) system where the analytical form of the Green's function is available. We then extend the validation to two 1D non-Hermitian systems with parity-time ($\mathcal{PT}$) symmetry [18,19], focusing on the Green's function at an exceptional point (EP). An EP is a unique degeneracy found only in non-Hermitian systems, where two or more eigenstates of the system coalesce. It has led to a plethora of intriguing phenomena, and in particular, it was shown recently that the Green's function can be fully decoupled from the coalesced eigenstate in a photonic system, which is instead given by the Jordan vector or the "missing dimension" of the Hilbert space [20]. We show that our method based on Eq. (2) captures this extraordinary behavior nicely in a ring cavity, besides describing correctly the Green's function in a $\mathcal{PT}$-symmetric photonic molecule. We further validate our method in quasi-1D waveguides, which are frequently employed to study disordered mesoscopic and optical systems [21–23]. In Sec. III, we first discuss how the defect state corresponding to the Green's function is conceptually different from previous studies of defect states, i.e., the corresponding defect strength is not an arbitrary parameter but uniquely determined by the Green's function itself. We then show that our approach based on Eq. (5) offers a systematic approach to construct a real eigenvalue for an arbitrary non-Hermitian system, without relying on the presence of $\mathcal{PT}$ symmetry or pseudo-Hermiticity [24]. This discussion also extends to a general $V(\mathbf{r}, \mathbf{r}')$ in Eq. (2), which replaces the δ function as a local or nonlocal potential. Finally, we highlight the intriguing manifestation of the linkage between the Green's function and a defect state in the aforementioned 2D topological lattice.

II. VALIDATION

A. 1D Hermitian case

We start with an example where the analytical form of the Green's function is available. Consider the scalar Helmholtz equation in 1D with a uniform refractive index $n \in \mathbb{R}$:

$$\mathcal{L} = -\frac{1}{n^2}\partial_x^2, \quad z = k^2. \tag{6}$$

Here k is the real-valued wave vector in free space. Below we take the speed of light in vacuum to be 1 and do not distinguish k from the (circular) frequency. We impose the Dirichlet boundary conditions $G(x, x') = 0$, $\psi_m(x) = 0$, at $x = 0, L$, which renders the system Hermitian. Consequently, it can be shown that the Green's function at the source position
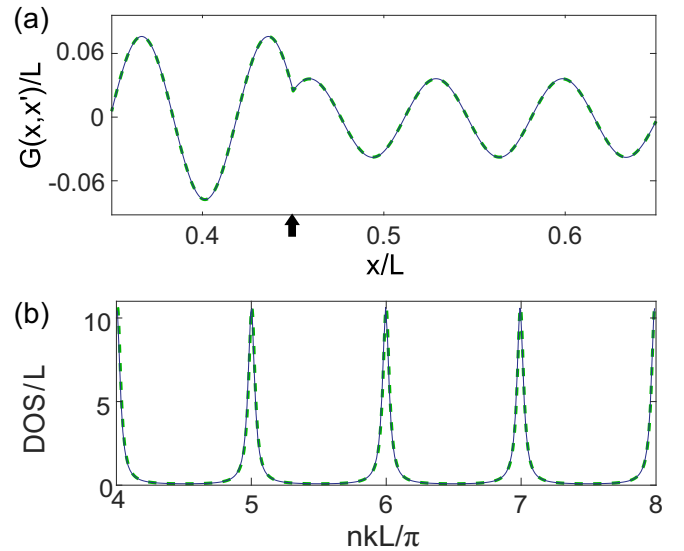

FIG. 1. The Green's function (a) and DOS (b) in a 1D dielectric cavity with perfect mirrors. The green dashed lines are obtained using the analytical expression (8), while the black solid lines are from our auxiliary eigenvalue approach (3). $n = 3$, $k = 30/L$, and $x' = 0.45L$ (marked by the arrow) are used in (a), and 2000 grid points are used for the finite-difference implementation of Eq. (2).

(i.e., λ_0^{-1}) is real:

$$\lambda_0 = \frac{k}{n}\left[\frac{1}{\tan[nk(x'-L)]} - \frac{1}{\tan(nkx')}\right]. \tag{7}$$

When solved using a finite-difference scheme [25], the numerical value of λ_0 given by Eq. (3) shows a good agreement with the analytical result given by Eq. (7). The corresponding Green's function, which we shown in Fig. 1(a), also agrees nicely with its analytical expression

$$G(x, x') = \begin{cases} \frac{\sin[nk(x-L)]}{\lambda_0 \sin[nk(x'-L)]} & (x > x'), \\ \frac{\sin(nkx)}{\lambda_0 \sin(nkx')} & (x \leqslant x'). \end{cases} \tag{8}$$

The numerical implementation of the δ function is usually taken to be the limit of a sharp analytical distribution, such as a Gaussian with the standard deviation $\sigma \to 0$. At the same time, another small quantity that requires attention in the finite-difference implementation of Eq. (2) is the lattice spacing Δx. If we choose $\sigma > \Delta x$, we find spurious eigenstates $\psi_{m \neq 0}(x)$ with almost identical spatial dependence away from the source position (not shown), but they have structures that reside in the finite extension of the approximated δ function (e.g., fast oscillations). This problem is remedied by letting $\sigma < \Delta x$, which practically leads to an approximation of the δ function that has a single non zero element at the position of the source, the value of which is given by $1/\Delta x$. This choice warrants that the integration of the δ function is 1 over any range enclosing the source and 0 otherwise. With this choice, we find that all spurious eigenvalues of Eq. (2) approach infinity (e.g., $|\lambda_{m \neq 0}L| > 10^{17}$ in the case shown in Fig. 1), and the sole, physical one λ_0 is easily obtained by setting the numerical routine to search for the eigenvalue with the smallest modulus.

As mentioned in the Introduction, our auxiliary eigenvalue approach also produces the LDOS directly. For a Hermitian system, a limiting procedure is needed to regulate the singularity at real-valued resonant frequencies:

$$\text{LDOS}(x; k) = \lim_{s \to 0^+} -\frac{2k}{\pi} \text{Im}[G(x, x; k + is)], \qquad (9)$$

i.e., a small positive imaginary part is added to the frequency here, constructing in this way the retarded Green's function [see Appendix A]. Equation (9) also applies to non-Hermitian cases, as long as the complex resonant frequencies are on or below the real axis. The integration of LDOS$(x; k)$ over the whole system then gives the density of states (DOS) as a function of the frequency.

To calculate DOS using our approach based on Eq. (2), we choose a small $s = 0.03/L$ and calculate $-\frac{2k}{\pi} \text{Im}[\lambda_0^{-1}]$ numerically. The result agrees well with the analytical result [see Fig. 1(b)], where λ_0 given by Eq. (7) is used. The latter leads to

$$\text{DOS}(k) = \sum_m \delta\left(k - \frac{m\pi}{nL}\right), \qquad (10)$$

as expected once $s \to 0$, where $k_m = m\pi/nL$ $(m = 1, 2 \ldots)$ are the real-valued resonant frequencies.

B. 1D non-Hermitian cases

For our next validation, we study the Green's function at an EP in a photonic molecule [26]. Such a case presents a serious challenge to the standard approach based on the eigenvalues of $\mathcal{L}$, i.e., the bilinear expansion

$$G(\mathbf{r}, \mathbf{r}'; z) = \sum_m \frac{\overline{\phi}_m(\mathbf{r}) \phi_m(\mathbf{r}')}{(z - z_m)(m, m)}, \qquad (11)$$

$$\mathcal{L}\phi_m(\mathbf{r}) = z_m \phi_m(\mathbf{r}). \qquad (12)$$

Depending on the symmetry of $\mathcal{L}$, the partner function $\overline{\phi}_m(\mathbf{r})$ may or may not be the same as $\phi_m^*(\mathbf{r})$, where "*" denotes the complex conjugation as usual. Here (m, n) is the resulting inner product of $\overline{\phi}_m(\mathbf{r})$ and $\phi_n(\mathbf{r})$. At an EP, the inner product (m, m) becomes zero due to the coalescence of two or more eigenstates of the system [19,27,28]. Although this divergence can be eliminated using a non-Hermitian perturbation theory [10,20], it requires *a priori* knowledge of the EPs and the Jordan chain, which adds to the complexity of the problem. Our auxiliary eigenvalue formulation, on the other hand, does not suffer from this drawback.

Below we exemplify our method and compare it to the result of a perturbation theory different from that mentioned above, which does not require the Jordan chain that completes the Hilbert space at the EP. Our photonic molecule is composed of two half-wavelength cavities coupled by a distributed Bragg reflector (DBR) placed in air [see Fig. 2(a), inset]. If different amounts of loss are introduced in the two half-wavelength cavities, an emerging effective $\mathcal{PT}$ symmetry governs the system [29].

Here we consider the outgoing boundary condition at a real-valued frequency, which corresponds to the laser and is different from quasibound states or resonances with a complex frequency throughout the entire space [30]. The resulting complex eigenvalues of $\mathcal{L}$ given in Eq. (6) are found
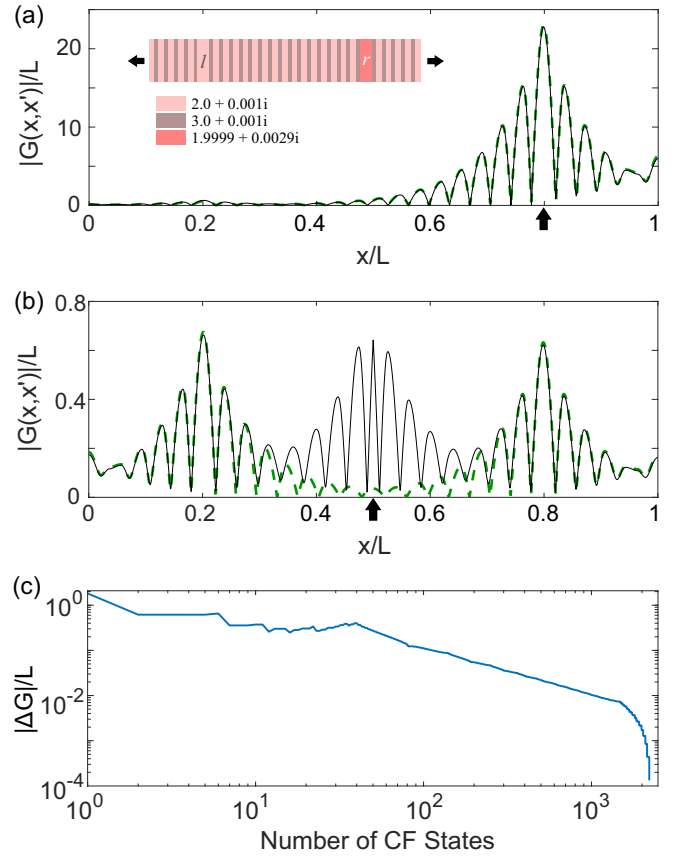

FIG. 2. Green's function of a $\mathcal{PT}$ photonic molecule at an EP. The source is placed at the center of the right cavity in (a) and in between the two cavities in (b). Inset in (a): Schematic of the photonic molecule and the imposed boundary condition, and labels denoting the refractive indices of each component of the heterostructure. Green dashed lines correspond to the perturbative expression in Eq. (16), and black solid lines correspond to our auxiliary eigenvalue approach. The locations of the sources are marked with arrows. (c) Difference between the bilinear expansion with the perturbative correction and the auxiliary method in (b) at the source position.

in the lower half of the complex frequency plane as a result of the non-Hermiticity caused by the cavity openness. These complex eigenvalues are known as continuous flux (CF) states [25,30], which have also been used to study nuclear decays [31,32]. We note that the EPs of CF states have not been studied before, unlike their counterparts of quasibound states or resonances.

In the vicinity of an EP of frequency k_0, the CF states in our system can be expressed in terms of waves confined in the left and right cavity, i.e., $\psi(x) \approx a_l \psi_l(x) + a_r \psi_r(x)$, where the amplitudes $a_{l,r}$ are determined by the Helmholtz equation. Without the $\mathcal{PT}$-symmetric perturbation, our photonic molecule is symmetric and hence $a_l = \pm a_r$ in the symmetric and antisymmetric modes, with CF frequencies $\tilde{k}_S, \tilde{k}_A$. The introduction of a weak $\mathcal{PT}$-symmetric perturbation in the dielectric function couples the amplitudes a_l and a_r, determined by their spatial overlap C with the non-Hermitian perturbation, which represents the strength of gain and loss.

The eigenfrequencies of the perturbed system are then found to be $q_{\pm}^2 = k_0^2(1 \pm \Delta_\varsigma)$. Here k_0 is the CF frequency of a single half-wavelength cavity sandwiched by two DBRs, and Δ is a dimensionless detuning defined by $(\tilde{k}_S^2 - \tilde{k}_A^2)/2k_0^2$. We have also defined $\varsigma \equiv \sqrt{1 - \beta^2}$, where $\beta = C/\Delta$. One EP is reached when $\varsigma = 0$, resulting in $q_{\pm}^2 = q_0^2$. The corresponding eigenstates $\psi_{\pm}(x)$ are given by

$$\psi_{\pm}(x) = \psi_l(x) + \beta_{\pm}\psi_r(x), \qquad (13)$$

where $\beta_{\pm} \equiv i\beta \pm \varsigma$. The inner product of the eigenstates is defined as

$$(i, j) \equiv \int \epsilon_0(x)\psi_i(x)\psi_j(x)dx, \quad (i, j = \pm), \qquad (14)$$

where $\epsilon_0(x)$ is the dielectric function before the $\mathcal{PT}$-symmetric perturbation is introduced. In other words, the partner functions in Eq. (11) are chosen as $\overline{\psi}_{\pm}(x) = \epsilon_0(x)\psi_{\pm}(x)$. This definition of the inner product warrants the biorthogonality $(+, -) = (-, +) = 0$, and we find $(+, +) = 2\beta_+\varsigma \to 0$, $(-, -) = -2\beta_-\varsigma \to 0$ as the system approaches the EP.

As seen from Eq. (11), the vanishing inner products $(+, +)$, $(-, -)$ here at the EP cause a catastrophe in the calculation of the Green's function, because the two corresponding terms diverge independent of the frequency:

$$G(x, x'; k) \approx \frac{\overline{\psi}_+(x')\psi_+(x)}{(q^2 - q_+^2)(+, +)} + \frac{\overline{\psi}_-(x')\psi_-(x)}{(q^2 - q_-^2)(-, -)}. \qquad (15)$$

However, it can be shown that the diverging behaviors in the two terms cancel each other precisely [10,20], leading to

$$G(x, x'; k) \approx \epsilon_0(x')\frac{\psi_l(x')\psi_l(x) + \psi_r(x')\psi_r(x)}{k^2 - k_0^2}$$
$$- i\Delta k_0^2 \epsilon_0(x')\frac{\psi_{EP}(x')\psi_{EP}(x)}{(k^2 - k_0^2)^2}, \qquad (16)$$

to the leading order of the small perturbation parameter ς. Here $\psi_{EP} = \psi_{\pm}|_{l=1}$ is the coalesced eigenstate at the EP. As expected [9,33], a second-order pole appears in the second term due to this coalescence. Details on the perturbative analysis can be found in Appendix B.

To verify the robustness of our method based on Eq. (3) in the vicinity of the EP, we choose the heterostructure of length L shown in Fig. 2. It consists of DBRs of refractive indexes $n_1 = 2 + 0.001i$ and $n_2 = 3 + 0.001i$, and each layer accommodates a quarter of their respective wavelengths at $ka = 1.570$, where a is the lattice constant. The two half-wavelength cavities with loss are fine-tuned to achieve an EP at $k_{EP}a = 1.570 - 0.006913i$ using $n_l = 2 + 0.001i$, $n_r = 1.9999 + 0.0029i$, and $k = \text{Re}[k_{EP}]$.

Figure 2 shows the Green's function of this system when the source is placed at different locations. First we place the source at the center of the right cavity, where we expect the approximation (16) using just $\psi_{\pm}(x)$ [and $\psi_{l,r}(x)$] to hold. As Fig. 2(a) shows, it is nearly identical to the result of our auxiliary eigenvalue approach (3), and the inclusion of more CF states away from the EP barely changes the Green's function (not shown). If instead we place the source at the center of the heterostructure, Eq. (16) alone is insufficient to
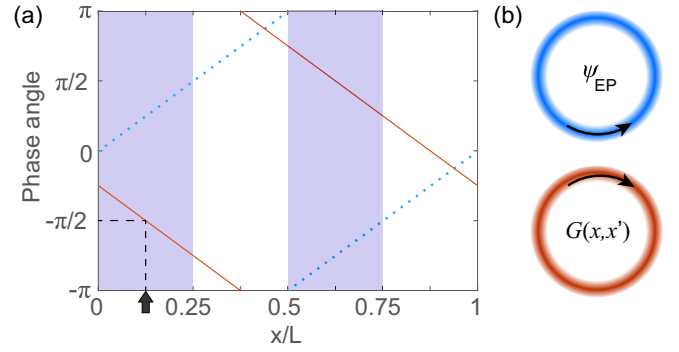

FIG. 3. Chirality-reversal Green's function in a $\mathcal{PT}$-symmetric ring cavity. (a) Phase of the Green's function (solid line) and the coalesced eigenstate (dotted line). Dashed lines point to the phase of the Green's function at the source (marked by the arrow). Shaded regions show the half periods with higher loss. (b) False color plots showing the constant amplitudes of the coalesced eigenstate (top) and the Green's function (bottom) along the ring. A finite width is imposed on the ring for visual clarity. Here $n_0 = 3$, $\delta n = 0.003$, $l = 1$, $k_{EP}L = 2.0944 - 0.0021i$, $kL = 2.0944$, and $x' = L/8$.

capture the features of the Green's function [see Fig. 2(b)]. However, once a large set of additional eigenfunctions of $\mathcal{L}$ are also included, a good agreement to our auxiliary eigenvalue approach is again observed [see Fig. 2(c)]. These results show that Eq. (3) provides a reliable and convenient method to calculate the Green's function, even in the presence of EPs.

A similar but more striking behavior of the Green's function at an EP was recently reported in an effective $\mathcal{PT}$-symmetric ring cavity with refractive index [20]

$$n(\theta) = (n_0 + i\delta n) + \delta n(\cos 2l\theta + i \sin 2l\theta). \qquad (17)$$

Here θ is the azimuthal angle, and below we will use the arc length $x = R\theta \in [0, L]$ as the coordinate, where R is the radius of the ring and $L = 2\pi R$ is the circumference. n_0 and δn are the real and imaginary parts of the background index, and the latter is positive to include both absorption and radiation losses. l is a positive integer, and the complex index grating, proportional to $e^{2il\theta}$, scatters the clockwise (CW) wave of angular momentum $-l$ to the counterclockwise (CCW) wave of angular momentum l but *not* vice versa. Note that the chirality and the sign of $\text{Im}[n]$ here are defined with respect to the temporal dependence $e^{-i\omega t}$.

Consequently, an EP appears at $k_{EP}R = l/(n_0 + i\delta n)$ with the coalesced CCW eigenstate $\psi(x) = e^{il\theta}$ [34]. The Green's function, on the other hand, can be fully decoupled from this mode even on resonance, if the source is placed at $\theta = (m + 1/4)\pi/l$ where m is a non-negative integer [20], i.e., at one of the most lossy spots in the passive ring cavity. The Green's function is given by the corresponding Jordan vector $J(x) \propto e^{-il\theta}$ instead, i.e., the "missing dimension" of the Hilbert space at the EP in the CW direction.

This extraordinary behavior is captured nicely using our auxiliary eigenvalue approach (see Fig. 3). In addition, a perturbative approach shows that the Green's function at the source is given by [20]

$$G(x', x'; k) \approx \frac{1}{2(k - k_{EP})k_{EP}L}, \qquad (18)$$

which is almost imaginary on resonance (i.e., $k = \mathrm{Re}[k_{\mathrm{EP}}]$) for a high-Q resonance with $|\mathrm{Im}[k_{\mathrm{EP}}]| \ll \mathrm{Re}[k_{\mathrm{EP}}]$. In the case shown in Fig. 3, this value is $(-113.99i + 0.228)R$ and nearly identical to that given by our auxiliary eigenvalue approach, i.e., $(-113.99i + 0.224)R$.

C. Quasi-1D waveguides

Quasi-1D waveguides are frequently used in the study of disordered mesoscopic and optical systems [21–23], and the Green's function plays a crucial role to construct the scattering and transfer matrices [35,36]. Here again we consider the scalar Helmholtz equation in a waveguide with background refractive index $n(\boldsymbol{r})$:

$$\mathcal{L} = -\frac{1}{n^2(\boldsymbol{r})}\big(\partial_x^2 + \partial_y^2\big), \quad z = k^2. \quad (19)$$

A finite width L_y in the transverse direction and the Dirichlet boundary conditions at $y = 0, L_y$ lead to a set of transverse modes ("channels") $f_m(y) = \sin[nk_m^{(y)}y]$, where $nk_m^{(y)} = m\pi/L_y$ is the transverse wave number and m is a positive integer. At a given frequency k, the longitudinal wave number in the mth channel is given by $nk_m^{(x)} = n\{k^2 - [k_m^{(y)}]^2\}^{1/2}$, and this channel is propagating (evanescent) if $k_m^{(x)}$ is real (imaginary).

To validate our auxiliary eigenvalue approach in quasi-1D waveguides, we first consider a uniform waveguide with the outgoing boundary condition. In this case an analytical expression exists for the Green's function, which can be written as the following infinite sum using the channel functions:

$$G(\boldsymbol{r}, \boldsymbol{r}'; k) = \sum_m n\frac{\sin\big[nk_m^{(y)}y'\big]\sin\big[nk_m^{(y)}y\big]}{ik_m^{(x)}L_y}e^{\pm ink_m^{(x)}x}. \quad (20)$$

Here the source point $\boldsymbol{r}' = (x', y')$ is placed at $x' = 0$, $y' \neq 0$, L_y, and the "$+ (-)$" sign in the exponent applies to a positive (negative) x. Clearly, only the propagating channels of a finite number affect the far-field behavior of the Green's function, while the logarithmic divergence of the Green's function at the source, a generic property in 2D (including quasi-1D), is reflected by the infinite number of evanescent channels in the summation. Numerically, this divergence is truncated either by the inclusion of only a finite number of evanescent channels or the finite resolution of the spatial discretization. We also note that the Green's function is dimensionless in quasi-1D.

Figure 4 shows one example where our auxiliary eigenvalue approach, implemented using the finite-difference method [25,37] (solid line), is compared with the analytical result given by Eq. (20). With just the three propagating channels available in this case (dotted line), Eq. (20) describes the Green's function well far from the source ($>2\,\mu\mathrm{m}$); with more channels included (e.g., 100, dashed line), a good agreement between Eq. (20) and our auxiliary eigenvalue approach is observed, where the grid spacings $\Delta x = 1/30\,\mu\mathrm{m}$, $\Delta y = 3/130\,\mu\mathrm{m}$ used in the finite-difference method are comparable to the shortest evanescent tail in the summation (i.e., $1/k_{m=100}^{(x)} \approx 0.01\,\mu\mathrm{m}$.)

For structured or disordered quasi-1D waveguides connected to two semi-infinite regions ("leads"), the Helmholtz equation is no longer separable in x and y, and an analytical
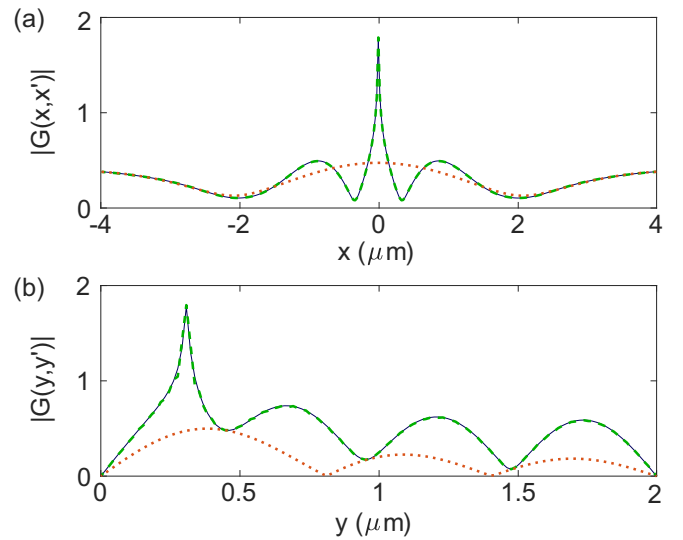

FIG. 4. Green's function in a uniform waveguide with $L_y = 2\,\mu\mathrm{m}$ and $n = 1.5$ everywhere. (a) and (b) show the slices along x and y at the source position $x' = 0$, $y' = 3/13\,\mu\mathrm{m}$. The free-space wavelength is 1550 nm.

expression for the Green's function in the form of Eq. (20) does not exist. Nevertheless, one can still compare to the bilinear expansion (11) as we show in Figs. 5(a) and 5(b) for a $\mathcal{PT}$-symmetric waveguide, despite its slow convergence [see Fig. 5(c)].

Here we also briefly review a standard technique used to calculate the Green's function in quasi-1D waveguides, i.e., the recursive Green's function method [38,39]. The comparison of the Green's functions obtained in our proposed approach and by the recursive Green's function method will be present in Sec. III.

The heart of the recursive Green's function method lies in the celebrated Dyson's equation:

$$\boldsymbol{G} = \boldsymbol{G}^0 + \boldsymbol{G}^0\boldsymbol{V}\boldsymbol{G}. \quad (21)$$

$\boldsymbol{G}$ is the Green's matrix expressed in the spatial basis here, i.e., its element $\boldsymbol{G}_{i,j}$ gives the value of the Green's function at point i when the source is placed at point j. In a quasi-1D system with N segments, $\boldsymbol{V}$ represents the couplings between the $(N-1)$th and Nth segments due to $\mathcal{L}$, and $\boldsymbol{G}^0$ is the value of $\boldsymbol{G}$ when $\boldsymbol{V}$ is taken to be zero. In other words, $\boldsymbol{G}^0$ contains the Green's matrices of two separate systems, one for the first $N-1$ segments on the left as a whole and one for the last segment on the right. This recursive procedure then starts with a single segment on the left and proceeds with more segments added from the right, one at a time.

When implemented using the finite-difference method that is equivalent to a tight-binding lattice [39], the recursive Green's function gives the identical result as our auxiliary eigenvalue approach, because they solve exactly the same discretized equation. Each segment of the system is simply a single column along y. We note, however, these two methods serve different purposes. The auxiliary eigenvalue approach gives the values of the Green's function inside the entire waveguide for a given position of the source, which can be both in the interior of the waveguide or on its boundaries. The
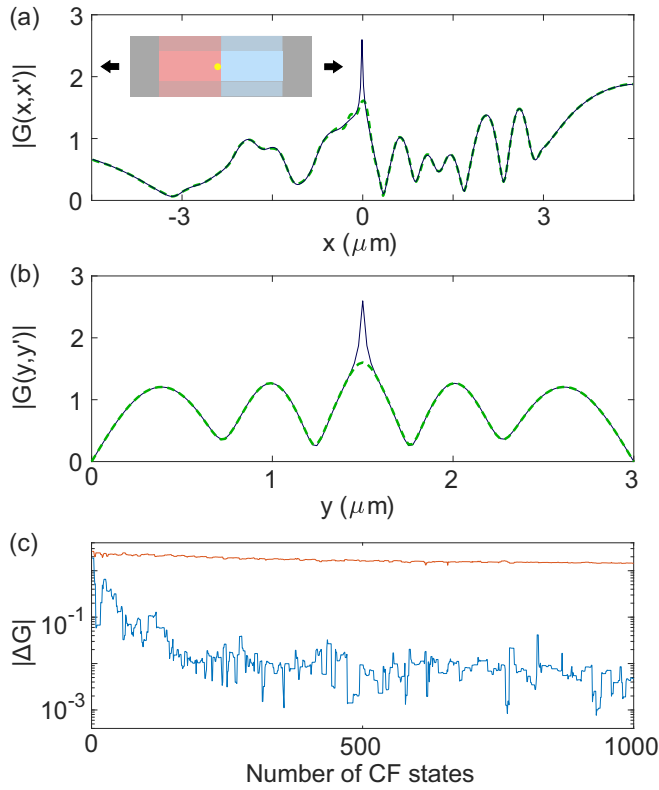
FIG. 5. (a, b) Same as Fig. 4 but for the Green's function in a $\mathcal{PT}$-symmetric waveguide. Here $L_x = 9\,\mu$m, $L_y = 3\,\mu$m, and the source is at $x' = -1/60\,\mu$m, $y' = 1.5\,\mu$m. Inset in (a): Schematic of the waveguide. $\text{Im}[n(x)] = \pm 0.05$ for $x \in [-3, 0]\,\mu$m and $[0, 3]\,\mu$m, respectively, where $\text{Re}[n(x)] = 2$ in the central half of the width. $\text{Re}[n(x)] = 1.2$ elsewhere inside the waveguide and 1 outside. (c) Convergence of the bilinear expansion at the source (upper) and at $x = 4.5\,\mu$m, $y = 1.5\,\mu$m (lower).

recursive Green's function method, on the other hand, is particularly suitable for solving the Green's function connecting the two boundary layers, with the source placed in either one of them [see Appendix C]. Extra steps are needed to solve the Green's function inside the waveguide, which is more intense numerically.

III. NEW INSIGHT

Having validated the proposed auxiliary eigenvalue approach to calculate the Green's function in various systems, we now turn to the insight this method provides, i.e., viewing the Green's function as a defect state as manifested by Eq. (5). Below we will discuss three essential aspects of this insight.

A. The Green's function determines its own defect strength

Unlike previous studies of defect states, the Green's function in our formalism corresponds to a *unique and only* eigenstate, instead of an (infinite) set of perturbed eigenstates of the original system described by $\mathcal{L}$ in Eq. (1). This difference is a manifestation of a more fundamental distinction between these two seemingly similar problems: the strength of the defect potential is a quantity that can be freely chosen
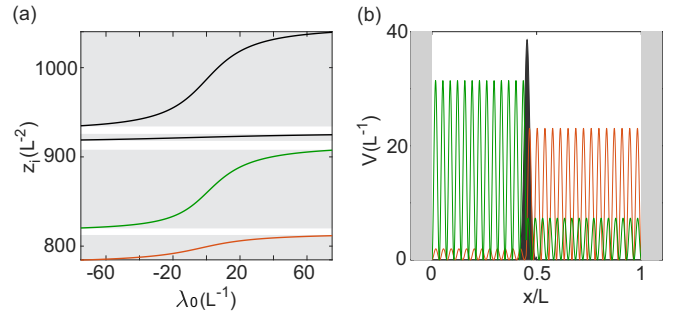

FIG. 6. (a) Eigenvalues of the Schrödinger equation (22) as a function of λ_0 for $n = 3$ and $x' = 0.45L$. Only four of them are shown near $z = 900/L^2$. (b) Schematics showing the potential as a function of the position. Shaded areas indicate the Dirichlet boundary condition and the δ-function potential with $\lambda_0 = 38.6/L$. Two unnormalized wave functions $|\psi(x)|^2$ are also shown.

in previous studies, while it is determined by the Green's function itself in our formalism.

To elucidate this point, we revisit the 1D Hermitian system described by the scalar Helmholtz equation in Fig. 1. The eigenstate $\psi_0(x)$ in our auxiliary eigenvalue equation (2) (and the Green's function) for a *given* energy $z = k^2$ then corresponds to the wave function of the following Schrödinger-like equation inside a closed box with a δ-function potential:

$$\left[-\frac{1}{n^2}\partial_x^2 + \lambda_0\delta(x - x')\right]\psi_0(x) = z\psi_0(x). \quad (22)$$

Previous studies of defect states would set the defect strength λ_0 as a free parameter and find all possible eigenvalues $\{z_i\}$ [see Fig. 6(a)]. This set, infinite in number in this case, corresponds to an infinite set of defect states, i.e., wave functions perturbed by the δ function [40].

When treating the Green's function as a defect state in our formalism, however, the defect strength λ_0 is not an arbitrary number. It is given by the inverse of the Green's function at the source position, as mentioned in the Introduction, i.e., it is *unknown* before the Green's function is solved. Such a problem has not emerged in previous studies of defect states, which has prevented a rigorous association of the Green's function as a defect state in the past.

Therefore, the fact that the Green's function determines its own defect strength is one important aspect of the insight that our formalism brings. Only after this defect strength is found via the Green's function itself can we relate previous studies of defect states to our result: the former seeks the one-to-infinite mapping between a given λ_0 and $\{z_i\}$, while the Green's function in our formalism is represented by a one-to-one mapping between z and λ_0. These two different mappings can be seen in Fig. 6(a), and it is important to note that the "bandwidths" of the eigenstates (gray shaded areas) do not overlap even when the range of λ_0 is extended from $-\infty$ to ∞. This feature is determined by the uniqueness of the Green's function: for a given energy z and source position x', the Green's function is uniquely determined by the boundary condition, and so is its inverse height at x' [i.e., λ_0; see Eq. (3) and its discussion]. Each of the "band gaps" in Fig. 6(a) (white areas) shrinks to a single point in this limit, and it corresponds

to one energy eigenvalue of either subsystem separated by the δ potential. Finally, we note that although the defect strength is unknown before the Green's function is solved, they can be found simultaneously in our approach as the generalized eigenvalue and eigenvector in Eq. (2).

B. Complex potential in non-Hermitian systems with real energy eigenvalues

In non-Hermitian systems, the energy eigenvalues $\{z_i\}$ are generally complex. However, there is a systematical way to construct real eigenvalues in non-Hermitian system, i.e., by involving $\mathcal{PT}$ symmetry [18], or equivalently, pseudo-Hermiticity [24]. In this approach, the energy eigenvalues appear either on the real axis or as complex conjugates.

The perspective we present here indicates another systematic way of finding real energy eigenvalue(s) in the presence of a complex potential. This observation is most obvious by inspecting Eq. (5) [and Eq. (22) in Sec. III A] with the understanding that the defect strength λ_0 is complex in general (see Sec. II B). Compared with the symmetry-based approach mentioned above, here we have a greater freedom to tailor such an energy eigenvalue, as we elucidate below.

As an example, let us consider the following 1D tight-binding lattice of a finite length N:

$$H\psi(n) = (-1)^{n-1}i\gamma\psi(n) + t[\psi(n+1) + \psi(n-1)]. \quad (23)$$

Here we have used the integer inside the parentheses to indicate the lattice site where the wave function ψ is evaluated. H can describe, for example, an array of optical cavities or waveguides with alternate on-site gain and loss. t in Eq. (23) is the nearest-neighbor coupling, and we have chosen the on-site energy z_0 of a single-cavity mode to be the reference energy and set it to be zero. With no detuning in the real part of the on-site energies and a real-valued t, this non-Hermitian system has non-Hermitian particle-hole (NHPH) symmetry [41–44]. The latter warrants a non-Hermitian flat-band [12] with $\text{Re}[z_i] = 0$ when the strength of gain and loss γ is above $2t$.

The Green's function of such a system is defined as

$$(z - H)G = \delta_{n'}, \quad (24)$$

i.e., it is a column vector parametrized by the energy z and the source position n'. $\delta_{n'}$ is an empty column except for the element 1 at the position n'. The corresponding auxiliary eigenvalue problem can be rewritten as

$$(H + \lambda_0 \Delta_{n'})\psi_0 = z\psi_0, \quad G = \frac{\psi_0}{\lambda_0 \psi_0(n')}, \quad (25)$$

where ψ_0 is the only eigenstate in the form of a column vector, and $\psi_0(n')$ is its value at the source position n'. Note that in a discrete system the column vector $\delta_{n'}$ becomes the matrix $\Delta_{n'}$ in Eq. (25), which has a single nonzero element in row n' and column n'.

If we now treat $H' \equiv H + \lambda_0 \Delta_{n'}$ as our target non-Hermitian Hamiltonian and seek one real eigenvalue of it by varying λ_0, we can simply assign any real number z to this target eigenvalue by solving λ_0 and ψ_0 simultaneously through Eq. (2) for this z. Figure 7(a) shows the required complex defect strength λ_0 when this real eigenvalue of H' is shifted
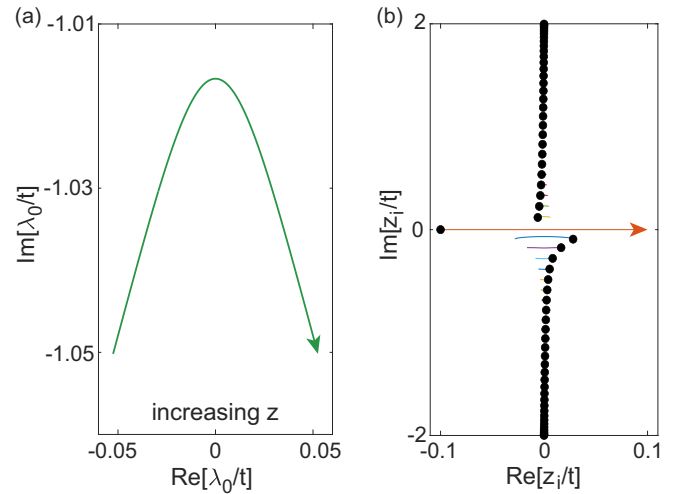

FIG. 7. (a) Trajectory of the complex defect strength λ_0 when z increases from $-t/10$ to $t/10$. The lattice has 60 sites with $n' = 1$ and $\gamma = 2t$. (b) Trajectories of all 60 eigenvalues of H' when λ_0 follows the trajectory in (a). Black dots show their values when $z = -t/10$. Only one of them is real, i.e., the one shifting from $-t/10$ to $t/10$ as designed.

from $-t/10$ to $t/10$. In this process, all other eigenvalues of H' remain complex, as shown by Fig. 7.

Importantly, this approach to realizing a real and tunable eigenvalue in non-Hermitian systems is not limited to the case with a (single) δ-function defect. We can replace the δ function [i.e., the matrix Δ'_n in Eq. (25)] by an arbitrary matrix V:

$$H'\psi_i = (H + \lambda_0 V)\psi_i = z_i\psi_i. \quad (26)$$

Here V represents a local (nonlocal) potential when it is diagonal (nondiagonal). To warrant a real eigenvalue z among the set of eigenvalues $\{z_i\}$ with a properly chosen λ_0, we solve the following generalized eigenvalue problem with the target $z \in \mathbb{R}$:

$$(z - H)\psi_m = \lambda_m V\psi_m. \quad (27)$$

This is exactly the discrete form of Eq. (2). We note that there is more than one pair of generalized eigenvalue λ_m and eigenstate ψ_m in Eq. (27), unless V represents a δ function [in which case the only pair $\{\lambda_0, \psi_0\}$ gives the Green's function via Eq. (25)]. This is a point we have made in the Introduction using the continuous operator $\mathcal{L}$.

Because there is now more than one generalized eigenvalue λ_m, any one of them can be chosen as the required potential strength λ_0 in Eq. (26). To illustrate this point, we revisit the 1D non-Hermitian system studied above and replace the δ function by a step function, whose value is 1 only in the left third of the lattice. Two possible trajectories of λ_0 (out of many) are shown in Fig. 8(a) using the procedure described above, each leading to the assigned real eigenvalue that is tuned from $-t/10$ to $t/10$ [Figs. 8(b) and 8(c)].
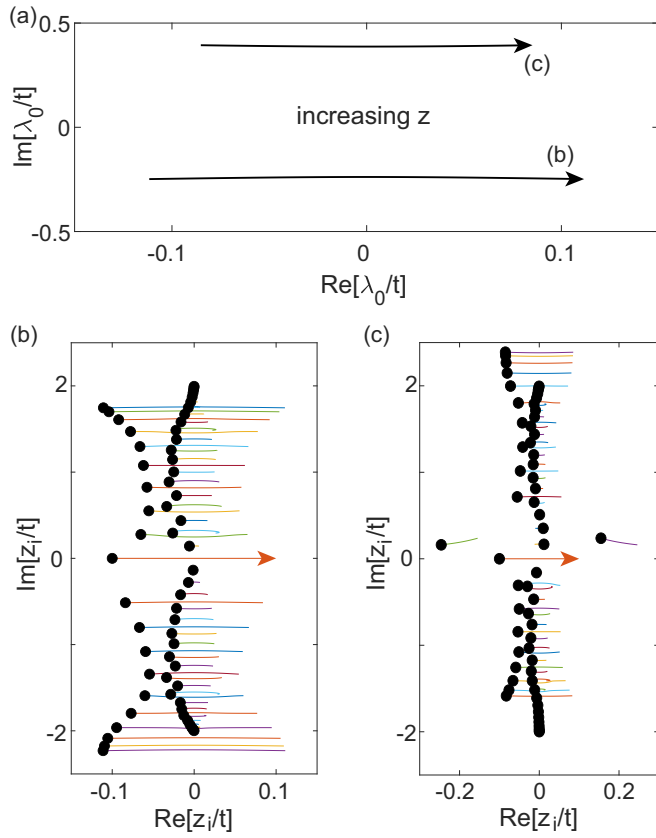
FIG. 8. (a) Same as Fig. 7(a) but with a different V mentioned in the text. Two possible trajectories of λ_0 are shown when the target real eigenvalue of H' in Eq. (26) is varied from $-t/10$ to $t/10$. All the trajectories of $\{z_i\}$ in this process are shown in (b) and (c), for each of the two curves in (a) respectively.

C. The Green's function as a topological edge state with a boundary defect

Finally, we reveal the most intriguing connection between the Green's function and a defect state, i.e., in a 2D topological lattice with a chiral edge state. While the zero eigenvalues of a spinor Green's function have been identified as a topological indicator [45], an intuitive understanding for the observation that the Green's function can behave as a chiral edge state circumventing the source position has been missing. Below we first briefly review the properties of such a system and lay out why this connection is striking.

This system breaks Lorentz reciprocity [46,47], which can be achieved in an electronic system by imposing a magnetic field. An analogy can be introduced to photonic systems by imposing an artificial gauge field, achieved experimentally by asymmetric couplings between two neighboring lattice sites on a tight-binding lattice [13–16]; while the couplings in both the x and y directions still have the same amplitude, their phases are now different. Here we consider a square lattice (Fig. 9) with uniform vertical coupling and horizontal asymmetric couplings of the same amplitude g, realizing a Landau gauge with a $\pi/2$ flux through the smallest plaquette [13,14]. Its bottom-right corner is pierced by the opposite flux, and an on-site potential shift of $-2g$ is also introduced to decouple it from the rest of the system. Due to its sublat-
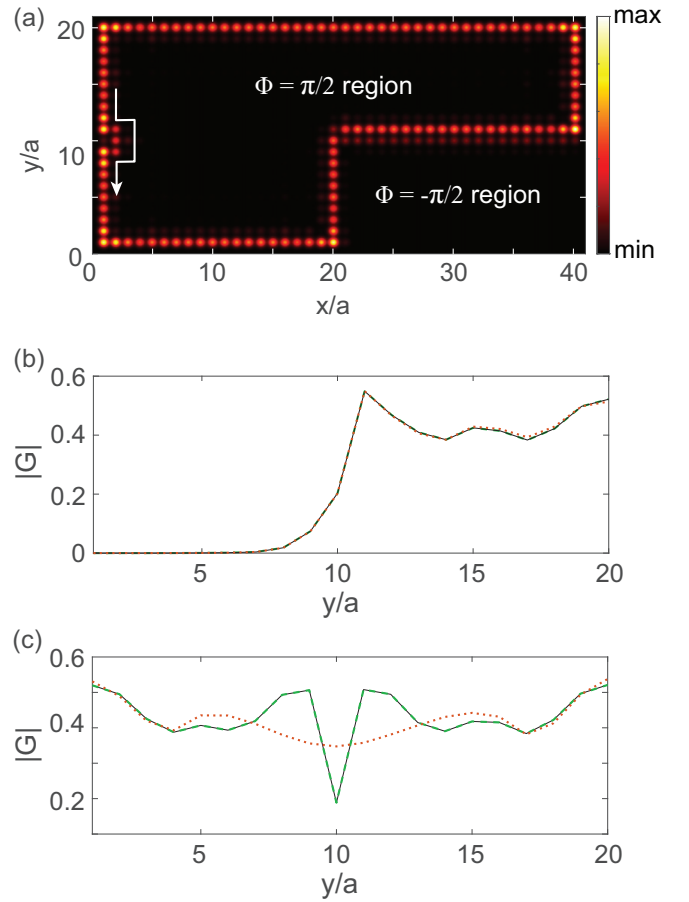

FIG. 9. Analogy between the Green's function and a chiral edge state circumventing a defect in a topological square lattice. (a) The Green's function calculated with $z = 1.85g$ and the source at $x = a$, $y = 10a$. (b), (c) Slices of the Green's function in (a) along y at $x = 40a$ and a, respectively. Solid, dashed, and dotted lines show the results of our auxiliary eigenvalue approach, the recursive Green's function, and the bilinear expansion with 20 chiral edge states in this band gap, respectively.

tice symmetry [48], the energy spectrum of the main region is symmetric about $z = 0$, set at the value of the identical on-site potential. It has an edge band with CCW chiral edge states in $z/g \in [1.08, 2.61]$, with their CW counterparts in $z/g \in [-2.61, -1.08]$.

When one places a source at the edge of the system which also has the frequency in one of the bulk band gaps, naively one would expect this source to couple to the chiral edge states in this bulk gap (as the bilinear expansion method indicates) and move smoothly around the edges of the two-dimensional defect-free system. This is indeed what we find on resonance, i.e., when z is almost the same as the energy of a chiral edge state of the unperturbed system (not shown). In this case, the Green's function is given essentially by this single chiral edge mode as the bilinear expansion suggests, and it goes through the defect created by the δ-function potential with little scattering. However, when the source is not on resonance with a chiral edge state, the resulting Green's function is smooth only *away* from the source position [see Fig. 9(a)], and an unexpected local minimum is found *at the source position*,

e.g., $x = a$, $y = 10a$ in Figs. 9(a) and 9(c), where $a = 1$ is the lattice constant.

Our approach offers an insight for this behavior: even though the system itself [represented by the operator $\mathcal{L}$ in Eq. (2)] does not have a defect, the Green's function is not trivially related to one of its eigenstates off resonance; instead, it is given by the eigenstate of a different system, with the introduction of a δ-function defect potential to the original, defect-free system. Even though the strength of this δ-function potential is unknown before the eigenvalue problem is solved, it is known that chiral edge states still exist in the presence of a boundary defect and circumvent the latter. This behavior is precisely what we find for the Green's function here as Fig. 9(a) shows, and its local minimum is hence the consequence of the topological protection of chiral edge states.

In this case, the δ-function defect creates a local perturbation so strong that it can only be captured by including a large number of unperturbed eigenstates of $\mathcal{L}$ in the bilinear expansion, including even chiral edge states in the opposite direction that are very different in energy (not shown). The far field, on the other hand, is only minutely affected by this local perturbation, and the bilinear expansion works well with a small number of unperturbed eigenstates of $\mathcal{L}$ in the same bulk gap [see Fig. 9(b)].

IV. DISCUSSION AND CONCLUSIONS

In summary, we have introduced in this work a perspective of the time-independent Green's function as a single eigenstate of an auxiliary eigenvalue formulation that embodies a defect state created by the δ-function potential. The height of the δ-function potential is determined by the inverse value of the Green's function at the source position, which is given directly in the form of a generalized eigenvalue problem given by Eq. (2). It is the only well-behaved and finite eigenvalue, easy to identify numerically. Therefore our approach differs both conceptually and computationally from previous investigations of eigenstates of a δ-function potential, which were not related to the Green's function.

The uniqueness of the eigenstate that gives the Green's function in our approach should be distinguished from the single bound state in an attractive 1D δ-function potential [49]. In our case the δ-function potential can be repulsive or attractive in a Hermitian system, depending on the sign of λ_0 [see Fig. 6(a) and Eq. (7)], and it becomes complex in general in non-Hermitian systems. Furthermore, the eigenstate in our approach does not depend on the original potential included in the operator $\mathcal{L}$, while the aforementioned bound state assumes a vacuum background. Finally, our eigenstate exists in higher dimensions as well, with clearly different boundary conditions and spatial profiles from a bound state [see Fig. 9(a), for example].

We have also verified the Green's function obtained in our method by comparing both to analytical results when available and to two frequently used numerical methods, i.e., the recursive Green's function method and the bilinear expansion in the basis of the system's eigenstates. At an EP, where a perturbative treatment of the bilinear expansion becomes necessary, our method is still robust, as seen from the examples in two $\mathcal{PT}$ systems. Our method also gives identical results to

the recursive Green's function method, implemented by finite difference on the same tight-binding lattice.

Our defect-state approach can also be applied to more numerically demanding cases, e.g., in the study of diffusive transport and wave localization [21,22]. We have investigated disordered quasi-1D waveguides over 100 wavelengths long and with over 60 transverse channels (not shown). In these cases, the memory storage for the recursive Green's function may become an issue, when the values of the Green's function in the interior of the waveguides are also computed for light-matter interaction or laser emissions. This is because the Green's matrix obtained from the recursive procedure mingles the values of the Green's function generated by sources placed across the entire system. The defect-state approach excels in this regard, because each source is treated independently. We should also mention that this advantage becomes less noticeable or even a disadvantage if the Green's function needs to be evaluated with the source at many different locations.

More importantly, our approach offers a previously unexplored physical insight that both the recursive Green's function method and the bilinear expansion lack, i.e., the linkage between the Green's function and a defect state. We have exemplified an intriguing manifestation of this linkage using a topological chiral edge state, where the local minimum of the Green's function is analogous to a chiral edge state circumventing a boundary defect. Therefore, even though our discussions have focused on the Helmholtz equation for scalar optical waves, we expect this perspective and the physical insight it offers to have important applications in other related fields as well, including condensed-matter systems, acoustics, electronic circuits, and so on.

APPENDIX A: RECIPROCITY IN THE AUXILIARY EIGENVALUE APPROACH

We derive some relations between the Green's functions $G(\mathbf{r}, \mathbf{r}')$ and $G(\mathbf{r}', \mathbf{r})$, based on the symmetries of $\mathcal{L}$. We start from a matrix description in which the Green's function operator $G(z)$ is defined from $G(\mathbf{r}, \mathbf{r}'; z) = \langle \mathbf{r}|G(z)|\mathbf{r}'\rangle$. We use the same symbol $\mathcal{L}$ for the matrix representation of the system. The Green's function satisfies the following equation:

$$[z\mathbf{1} - \mathcal{L}]G(z) = \mathbf{1}, \quad G(z)[z\mathbf{1} - \mathcal{L}] = \mathbf{1}, \quad \text{(A1)}$$

where $\mathbf{1}$ is the identity matrix. Here, we identify the Green's function as being both the right and left matrix inverses of $[z\mathbf{1} - \mathcal{L}]$. Considering that in non-Hermitian physics there is a distinction between left and right sets of eigenvectors [50], one may attempt to distinguish between the left and right Green's functions. However, it can be shown that they are identical, since $[z\mathbf{1} - \mathcal{L}]$ is a matrix of full rank. It is possible to obtain relations between $G(z)$ and $[G(z)]^T$, or $[G(z)]^\dagger$, when performing matrix transposition or Hermitian conjugation on Eq. (A1).

We start by analyzing the case $\mathcal{L}^T = \mathcal{L}$: matrix transposition of Eq. (A1) leads to the relation $G(z)^T = G(z)$, or more explicitly, $G(\boldsymbol{r}', \boldsymbol{r}; z) = G(\boldsymbol{r}, \boldsymbol{r}'; z)$, which is the usual Lorentz reciprocity condition. This relation holds when $\mathcal{L}$ is a symmetric matrix, describing a system with symmetric couplings and hence without an effective magnetic field. It is valid for non-Hermitian systems with this property as well, such as the case with a non-Hermitian flatband discussed in Fig. 7 of the main text.

In a general Hermitian system, $\mathcal{L}^\dagger = \mathcal{L}$, and uniqueness of the matrix inverse demands that $[G(z)]^T = [G(z^*)]^*$, or $G(\boldsymbol{r}', \boldsymbol{r}; z) = [G(\boldsymbol{r}, \boldsymbol{r}'; z^*)]^*$. It is customary to state this relation in terms of Green's functions $G^{(\pm)}$ with *outgoing* and *incoming* boundary conditions, respectively. This nomenclature is especially useful if $z = k + i\eta$, with $\eta > 0$ small compared to k:

$$G^{(\pm)}(\boldsymbol{r}, \boldsymbol{r}'; k) \equiv \lim_{\eta \to 0^+} G(\boldsymbol{r}, \boldsymbol{r}'; k \pm i\eta). \quad (A2)$$

Therefore we can write the reciprocity condition as $G^{(\pm)}(\boldsymbol{r}', \boldsymbol{r}; k) = [G^{(\mp)}(\boldsymbol{r}, \boldsymbol{r}'; k)]^*$. The solutions $G^{(\pm)}$ are oftentimes referred to as the *retarded* and *advanced* Green's functions, inspired from the association to sources generating outgoing or incoming waves. Systems that are non-Hermitian and do not have symmetric couplings lead to more complicated reciprocity relations, involving the Green's functions of two different systems. This is expected, since the scattering properties derived from the Green's functions of systems related by a time-reversal transformation are nontrivial and yet to be understood. Reference [51] provides interesting scattering relations between two "time-reversal partners" in 1D and quasi-1D systems.

Our Green's function approach for time-reversal or non-Hermitian symmetric systems leads to a relation between the single eigenstates:

$$\frac{\psi_0(\boldsymbol{r}, \boldsymbol{r}')}{\lambda_0(\boldsymbol{r}')\psi_0(\boldsymbol{r}', \boldsymbol{r}')} = \frac{\psi_0(\boldsymbol{r}', \boldsymbol{r})}{\lambda_0(\boldsymbol{r})\psi_0(\boldsymbol{r}, \boldsymbol{r})}, \quad (A3)$$

or

$$\psi_0(\boldsymbol{r}', \boldsymbol{r}) = \psi_0(\boldsymbol{r}, \boldsymbol{r}')\left[\frac{\lambda_0(\boldsymbol{r})\psi_0(\boldsymbol{r}, \boldsymbol{r})}{\lambda_0(\boldsymbol{r}')\psi_0(\boldsymbol{r}', \boldsymbol{r}')}\right], \quad (A4)$$

whereas for the general non-Hermitian problem, we find

$$\bar{\psi}_0(\boldsymbol{r}', \boldsymbol{r}) = [\psi_0(\boldsymbol{r}, \boldsymbol{r}')]^*\left[\frac{\bar{\lambda}_0(\boldsymbol{r})\bar{\psi}_0(\boldsymbol{r}, \boldsymbol{r})}{\lambda_0(\boldsymbol{r}')\psi_0(\boldsymbol{r}', \boldsymbol{r}')}\right], \quad (A5)$$

where we used the notation $\bar{\psi}_0(\boldsymbol{r}, \boldsymbol{r}', z) \equiv \psi_0(\boldsymbol{r}, \boldsymbol{r}', z^*)$. The same result is obtained if we identify $\bar{\psi}_0$ with the advanced solution and ψ_0 with the retarded solution, or vice versa.

APPENDIX B: PERTURBATION THEORY AT AN EP

Below we review a generic procedure to approach effective $\mathcal{PT}$-symmetric systems with the outgoing boundary condition based on the coupled-mode theory. In particular, we describe a photonic molecule that consists of identical components $\mathbb{L}$ and $\mathbb{R}$ that support localized states $\psi_l(x)$ and $\psi_r(x)$ in each component. The system can be, for instance, two identical whispering gallery resonators that are brought to proximity such that their modes overlap and produce a pair of bonding

and antibonding states. Alternatively, one can think of a pair of half-wavelength cavities coupled by a DBR, which is the system discussed in Sec. II B of the main text. Note that due to the outgoing boundary condition, such systems are not truly $\mathcal{PT}$ symmetric, because time reversal changes the outgoing boundary condition to the incoming boundary condition. However, if the states are highly localized, as in our discussion below, the minute flux in or out of the system can be omitted in the discussion of the coupled-mode theory.

The left component satisfies the Helmholtz equation:

$$\left[\partial_x^2 + \epsilon_l(x)k_0^2\right]\psi_l(x) = 0 \quad (x \in \mathbb{L}), \quad (B1)$$

$$\left[\partial_x^2 + k^2\right]\psi_l(x) = 0 \quad (x \in \text{elsewhere}). \quad (B2)$$

Here k is the real-valued external frequency at which the Green's function is going to be evaluated, and $k_0 \sim k$ is one complex-valued CF frequency. The right component is defined similarly, and the localized states are normalized by $\int_{x \in \mathbb{L}, \mathbb{R}} \epsilon_{l,r}\psi_{l,r}^2 dx = 1$, respectively. The composite system is defined by $\epsilon_0(x) = \epsilon_l(x) + \epsilon_r(x)$ and satisfies

$$\left[\partial_x^2 + \epsilon_0(x)\tilde{k}^2\right]\tilde{\psi}(x) = 0 \quad (x \in \mathbb{L} \cup \mathbb{R}), \quad (B3)$$

$$\left[\partial_x^2 + k^2\right]\tilde{\psi}(x) = 0 \quad (x \in \text{elsewhere}), \quad (B4)$$

where $\tilde{k}$ is the CF frequency of a "supermode"

$$\tilde{\psi}(x) = a_l\psi_l(x) + a_r\psi_r(x), \quad (B5)$$

to be determined. We note that $\tilde{\psi}(x)$ automatically satisfies the outgoing boundary condition at the two ends of the composite system due to the same property of both $\psi_{l,r}(x)$.

We make the following assumption about the system: the spatial overlapping of the localized states in one cavity is very weak, i.e., $\int_{x \in \mathbb{L}, \mathbb{R}} \epsilon_{l,r}\psi_l\psi_r dx \equiv g$ ($|g| \ll 1$). In addition, we note that the frequency shift due to $|\int_{x \in \mathbb{R}} \epsilon_r\psi_l^2 dx| = |\int_{x \in \mathbb{L}} \epsilon_l\psi_r^2 dx|$ is even smaller, which is then neglected in our analysis below.

To derive the coupled-mode theory, we first insert Eq. (B5) into Eqs. (B3), (B4) and simplify the result using Eqs. (B1), (B2) for $\psi_l(x)$ and their counterparts for $\psi_r(x)$. Then we multiply the resulting equation by either $\psi_l(x)$ or $\psi_r(x)$ and perform an integration in the left and right component of the system, respectively, obtaining in this way two independent equations:

$$\begin{bmatrix} \tilde{k}^2 - k_0^2 & g\tilde{k}^2 - tk^2 \\ g\tilde{k}^2 - tk^2 & \tilde{k}^2 - k_0^2 \end{bmatrix}\begin{bmatrix} a_l \\ a_r \end{bmatrix} = 0. \quad (B6)$$

It is a system of equations for the unknown amplitudes $a_{l,r}$ and frequency $\tilde{k}$, where t is defined by $\int_{x \in \mathbb{L}} \psi_r^2 dx = \int_{x \in \mathbb{R}} \psi_l^2 dx$. Since the matrix operator is symmetric and has identical diagonal elements, a zero-determinant condition implies that $a_r = \pm a_l$, giving rise to the *symmetric* and *antisymmetric* modes $\tilde{\psi}_S(x)$ and $\tilde{\psi}_A(x)$ respectively, with frequencies

$$\tilde{k}_{S,A}^2 = \frac{k_0^2 \pm tk^2}{1 \pm g}. \quad (B7)$$

With the aforementioned approximations $|g| \ll 1$ and $k_0 \sim k$, these frequencies reduce to

$$\tilde{k}_S^2 \approx (1 + t - g)k_0^2, \quad \tilde{k}_A^2 \approx (1 - t + g)k_0^2, \quad (B8)$$

and their splitting is equal to $\tilde{k}_S^2 - \tilde{k}_A^2 = 2(t-g)k_0^2 \equiv 2\Delta k_0^2$.

Now we introduce a $\mathcal{PT}$-symmetric perturbation $i\epsilon_1(x)$, which is an odd function of x. The effective $\mathcal{PT}$-symmetric system satisfies

$$\left[\partial_x^2 + (\epsilon_0(x) + i\epsilon_1(x))q^2\right]\psi(x) = 0, \qquad \text{(B9)}$$

where q is the perturbed CF frequency to be determined together with the amplitudes A and S in the expansion of the perturbed eigenstate $\psi(x) = A\tilde{\psi}_A(x) + S\tilde{\psi}_S(x)$. Following an analogous procedure to that described above, we obtain again a system of equations that can be represented by the following matrix equation for A, S:

$$\begin{bmatrix} q^2 - \tilde{k}_S^2 & iCq^2 \\ iCq^2 & q^2 - \tilde{k}_A^2 \end{bmatrix}\begin{bmatrix} S \\ A \end{bmatrix} = 0, \qquad \text{(B10)}$$

where $C \equiv \int \epsilon_1(x)\tilde{\psi}_A(x)\tilde{\psi}_S(x)dx$ is integrated over the whole system. We note that this equation and the following perturbative results apply when $\epsilon_0(x)$ is complex, i.e., the system does not need to have balanced gain and loss to be effectively $\mathcal{PT}$ symmetric [52].

To rewrite it in a more familiar form, we note that since the $\mathcal{PT}$-symmetric perturbation is assumed to be weak, we

approximate Cq^2 by Ck_0^2, which leads to

$$\tilde{H}\begin{bmatrix} S \\ A \end{bmatrix} \equiv \begin{bmatrix} k_S^2 & -iCk_0^2 \\ -iCk_0^2 & k_A^2 \end{bmatrix}\begin{bmatrix} S \\ A \end{bmatrix} = q^2\begin{bmatrix} S \\ A \end{bmatrix}. \qquad \text{(B11)}$$

The perturbed frequency q is then found to be

$$q_\pm^2 \approx k_0^2(1 \pm \sqrt{\Delta^2 - C^2}), \qquad \text{(B12)}$$

where we have used the forms of $\tilde{k}_{S,A}^2$ from Eq. (B8). The EP then emerges when $C^2 = \Delta^2$, where $q_\pm \equiv k_{EP} \approx k_0$. In the main text we have introduced $\varsigma \equiv \sqrt{1 - \beta^2}$ and $\beta \equiv C/\Delta$.

This system of equations can be transformed to the basis of left and right components, in terms of the amplitudes a_l, a_r:

$$H\begin{bmatrix} a_l \\ a_r \end{bmatrix} \equiv k_0^2\begin{bmatrix} 1 - iC & \Delta \\ \Delta & 1 + iC \end{bmatrix}\begin{bmatrix} a_l \\ a_r \end{bmatrix} = q^2\begin{bmatrix} a_l \\ a_r \end{bmatrix}. \qquad \text{(B13)}$$

It has the most familiar form of a $\mathcal{PT}$-symmetric Hamiltonian. This is the model that we have used to describe the photonic molecule in Sec. II B.

The perturbative result of the Green's function given by Eq. (16) in the main text is derived from the following expression:

$$G(x, x'; k) = \frac{\epsilon_0(x')}{\left(k^2 - k_0^2\right)^2 - \Delta^2\varsigma^2}\Big\{\left(k^2 - k_0^2\right)[\psi_l(x')\psi_l(x) + \psi_r(x')\psi_r(x)]$$

$$- \Delta k_0^2[\,i\beta[\psi_l(x')\psi_l(x) - \psi_r(x')\psi_r(x)] - [\psi_l(x')\psi_r(x) + \psi_r(x')\psi_l(x)]\,]\Big\}, \qquad \text{(B14)}$$

by dropping terms proportional to ς^2, including that in $\beta = \sqrt{1 - \varsigma^2} \approx 1$. We note that Eq. (B14) includes terms to all orders of ς. Here it is unnecessary to invoke the Jordan vector $J(x)$ that completes the Hilbert space at the EP [20], but to compare with the result given in Ref. [10], we note that it can be chosen as

$$J(x) = \frac{i\psi_l(x) + \psi_r(x)}{2\sqrt{\Delta}k_0}e^{-i\pi/4}, \qquad \text{(B15)}$$

which satisfies

$$\left[H - k_{EP}^2\mathbf{1}\right]J(x) = \psi_{EP}(x) \qquad \text{(B16)}$$

with the coalesced eigenstate

$$\psi_{EP}(x) = 2\sqrt{\Delta}k_0e^{-i\pi/4}[\psi_l(x) + i\psi_r(x)] \qquad \text{(B17)}$$

at the EP. Here $\mathbf{1}$ is the identity matrix, and $\psi_{EP}(x)$ is normalized differently from the main text to satisfy $(\psi_{EP}, J) = 1$ [see the definition of the inner product given by Eq. (14) in the main text]. We further note that the $\mathcal{PT}$-symmetric Hamiltonian given by Eq. (B13) above is symmetric, and hence it is unnecessary to distinguish left and right eigenstates (and Jordan vectors) because they are identical. Using $J(x)$ and $\psi_{EP}(x)$ specified above, we find that the Green's function derived in Ref. [10] at the EP agrees with our result given by Eq. (16) in the main text, once the additional factor $\epsilon_0(x')$ is accounted for that originates from rewriting the Helmholtz equation as Eq. (6) in the main text.

APPENDIX C: THE RECURSIVE GREEN'S FUNCTION

Below we briefly review the recursive Green's function method and our implementation of it using finite difference. Assuming that the Green's function defined by Eq. (1) has been obtained at every grid point for a quasi-1D waveguide with $N - 1$ columns and N_y rows, we can write down a Green's matrix $\mathbf{G}^{(N-1)}$ that satisfies

$$[z\mathbf{1}^{(N-1)} - \mathbf{L}^{(N-1)}]\mathbf{G}^{(N-1)} = \mathbf{1}^{(N-1)}. \qquad \text{(C1)}$$

Its individual element $\mathbf{G}_{i,j}^{(N-1)}$ gives the value of the Green's function at point i when the source is placed at point j. We reserve the notation $\mathbf{G}_{i,j}^{(N-1)}$ without the underscore below the subscripts for the $N_y \times N_y$ block of the Green's matrix evaluated in the ith column with the source in the jth column, and we apply the same notation to other matrices as well. The $(N - 1)N_y$ grid points are labeled from the first to the last point in the first column, continued in the same way onto the second and remaining columns. $\mathbf{1}^{(N-1)}$ is the identity matrix with $(N - 1)N_y$ rows and columns, and $\mathbf{L}^{(N-1)}$ is the finite-difference implementation of the operator $\mathcal{L}$ in Eq. (1), again with $(N - 1)N_y$ rows and columns.

To calculate the Green's matrix with an additional column added from the right, we separate $\mathbf{L}^{(N)}$ into $\mathbf{L}^0 + \mathbf{V}$ and construct an ancillary matrix $\mathbf{G}^0$, where

$$\mathbf{L}^0 \equiv \begin{pmatrix} \mathbf{L}^{(N-1)} & \\ & \mathbf{L}_{N,N}^{(N)} \end{pmatrix}, \quad \mathbf{G}^0 \equiv \begin{pmatrix} \mathbf{G}^{(N-1)} & \\ & \mathbf{G}_{N,N}^0 \end{pmatrix}.$$

V only contains the couplings between the $(N-1)$th and Nth columns in $L^{(N)}$, and

$$[z\mathbf{1}^{(1)} - L_{N,N}^{(N)}]G_{N,N}^0 = \mathbf{1}^{(1)} \tag{C2}$$

defines the Green's matrix $G_{N,N}^0$ of the isolated Nth column. It is straightforward to show that

$$[z\mathbf{1}^{(N)} - L^0]G^0 = \mathbf{1}^{(N)}, \tag{C3}$$

and we derive the well-known Dyson's equation

$$G^{(N)} = G^0 + G^{(N)}VG^0, \tag{C4}$$

where $G^{(N)}$ is defined by

$$[z\mathbf{1}^{(N)} - L^{(N)}]G^{(N)} = \mathbf{1}^{(N)}, \tag{C5}$$

similar to Eq. (C1). Equation (C4) can be verified directly by multiplying $[z\mathbf{1}^{(N)} - L^{(N)}]$ from the left.

Below we drop the superscript of $G^{(N)}$. Equation (C4) differs from its more familiar form in mesoscopic physics [39], i.e.,

$$\tilde{G} = \tilde{G}^0 + \tilde{G}^0 V\tilde{G}, \tag{C6}$$

because there the Green's matrix is defined by $\tilde{G}[z\mathbf{1}^{(N)} - L^{(N)}] = \mathbf{1}^{(N)}$ instead. We have already proven the equivalence between the left and right matrix inverses of $[z\mathbf{1} - \mathcal{L}]$ in Appendix A, thus $\tilde{G}$ and G are identical.

Using Eq. (C4), the recursive relations between the blocks of the Green's matrices $G_{i,j}$ connecting the two boundary layers (i.e., the 1st and Nth columns) can be derived:

$$G_{NN} = A^{-1}, \tag{C7}$$

$$G_{1N} = G_{1,N-1}^0 V_{N-1,N}A^{-1}, \tag{C8}$$

$$G_{N1} = G_{N,N}^0 V_{N,N-1}G_{N-1,1}^0, \tag{C9}$$

$$G_{11} = G_{1,1}^0 + G_{1,N}V_{N,N-1}G_{N-1,1}^0. \tag{C10}$$

A single matrix inversion for

$$A = z\mathbf{1}^{(1)} - L_{N,N}^{(N)} - V_{N,N-1}G_{N-1,N-1}^0 V_{N-1,N} \tag{C11}$$

is needed when adding one layer from the right, and its last term is often referred to as the self-energy [38]. Note that besides the operator $L^{(N)}$, all the pieces of information needed for this recursive scheme are the same four matrix for the system with $(N-1)$ layers. As a result, the recursive Green's function method is highly efficient to treat transport problems, which does not require the knowledge of the Green's function inside the system. If we need the full Green's matrix to investigate, for example, light-matter interaction in the bulk of the system, more steps are required in the recursive Green's function, which scale as N^2 and are more intense numerically.

[1] I. Stakgold and M. Holst, *Green's Functions and Boundary Value Problems*, Pure and Applied Mathematics (John Wiley & Sons, Hoboken, NJ, 2011), 3rd ed.

[2] Y. A. Melnikov and V. N. Borodin, *Green's Functions*, no. 48 in Developments in Mathematics (Springer, Cham, 2017).

[3] P. M. Morse and H. Feshbach, *Methods of Theoretical Physics* (McGraw-Hill, New York, 1953), Vol. 1.

[4] G. Green, *Mathematical Papers of the Late George Green* (Macmillan, London, 1871).

[5] J. Schwinger, *Particles, Sources, and Fields* (Perseus, Reading, MA, 1998).

[6] G. Rickayzen, *Green's Functions and Condensed Matter* (Academic Press, New York, 1980).

[7] E. Economou, *Green's Functions in Quantum Physics* (Springer, New York, 2007), 3rd ed.

[8] M. Davy, Z. Shi, J. Wang, X. Cheng, and A. Z. Genack, Phys. Rev. Lett. **114**, 033901 (2015).

[9] Z. Lin, A. Pick, M. Lončar, and A. W. Rodriguez, Phys. Rev. Lett. **117**, 107402 (2016).

[10] A. Pick, B. Zhen, O. D. Miller, C. W. Hsu, F. Hernandez, A. W. Rodriguez, M. Soljačić, and S. G. Johnson, Opt. Express **25**, 12325 (2017).

[11] R. G. Newton, *Scattering Theory of Waves and Particles* (Springer, Berlin, 1982), 2nd ed.

[12] B. Qi, L. Zhang, and L. Ge, Phys. Rev. Lett. **120**, 093901 (2018).

[13] M. Hafezi, E. A. Demler, M. D. Lukin, and J. M. Taylor, Nat. Phys. **7**, 907 (2011).

[14] M. Hafezi, S. Mittal, J. Fan, A. Migdall, and J. M. Taylor, Nat. Photonics **7**, 1001 (2013).

[15] M. A. Bandres, S. Wittek, G. Harari, M. Parto, J. Ren, M. Segev, D. N. Christodoulides, and M. Khajavikhan, Science **359**, eaar4005 (2018).

[16] H. Zhao, X. Qiao, T. Wu, B. Midya, S. Longhi, and L. Feng, Science **365**, 1163 (2019).

[17] S. Barik, A. Karasahin, C. Flower, T. Cai, H. Miyake, W. DeGottardi, M. Hafezi, and E. Waks, Science **359**, 666 (2018).

[18] C. M. Bender and S. Boettcher, Phys. Rev. Lett. **80**, 5243 (1998).

[19] L. Feng, R. El-Ganainy, and L. Ge, Nat. Photonics **11**, 752 (2017).

[20] H. Z. Chen, T. Liu, H. Y. Luan, R. J. Liu, X. Y. Wang, X. F. Zhu, Y. B. Li, Z. M. Gu, S. J. Liang, H. Gao *et al.*, Nat. Phys. **16**, 571 (2020).

[21] C. W. J. Beenakker, Rev. Mod. Phys. **69**, 731 (1997).

[22] Y. Imry, *Introduction to Mesoscopic Physics*, 2nd ed. (Oxford University Press, Oxford, 2008).

[23] P. A. Mello and N. Kumar, *Quantum Transport in Mesoscopic Systems* (Oxford University Press, Oxford, England, 2004).

[24] A. Mostafazadeh, J. Math. Phys. **43**, 205 (2002).

[25] L. Ge, Photonics Res. **5**, B20 (2017).

[26] M. Liertzer, L. Ge, A. Cerjan, A. D. Stone, H. E. Türeci, and S. Rotter, Phys. Rev. Lett. **108**, 173901 (2012).

[27] W. D. Heiss, J. Phys. A **37**, 2455 (2004).

[28] M. V. Berry, Czech. J. Phys. **54**, 1039 (2004).

[29] L. Ge and R. El-Ganainy, Sci. Rep. **6**, 24889 (2016).

[30] H. E. Türeci, A. D. Stone, and B. Collier, Phys. Rev. A **74**, 043822 (2006).

[31] P. L. Kapur and R. Peierls, Proc. Roy Soc. A **166**, 277 (1938).

[32] M. L. Goldberger and K. M. Watson, Phys. Rev. **136**, B1472 (1964).

[33] W. D. Heiss, Int. J. Theor. Phys. **54**, 3954 (2015).

[34] P. Miao, Z. Zhang, J. Sun, W. Walasik, S. Longhi, N. M. Litchinitser, and L. Feng, Science **353**, 464 (2016).

[35] D. S. Fisher and P. A. Lee, Phys. Rev. B **23**, 6851 (1981).

[36] A. D. Stone and A. Szafer, IBM J. Res. Dev. **32**, 384 (1988).

[37] L. Ge, K. G. Makris, D. N. Christodoulides, and L. Feng, Phys. Rev. A **92**, 062135 (2015).

[38] D. J. Thouless and S. Kirkpatrick, J. Phys. C **14**, 235 (1981).

[39] F. Sols, M. Macucci, U. Ravaioli, and K. Hess, J. Appl. Phys. **66**, 3892 (1989).

[40] S. H. Patil, Eur. J. Phys. **27**, 899 (2006).

[41] S. Malzard, C. Poli, and H. Schomerus, Phys. Rev. Lett. **115**, 200402 (2015).

[42] L. Ge, Phys. Rev. A **95**, 023812 (2017).

[43] J. D. H. Rivero and L. Ge, Phys. Rev. B **103**, 014111 (2021).

[44] K. Kawabata, S. Higashikawa, Z. Gong, Y. Ashida, and M. Ueda, Nature Commun. **10**, 297 (2019).

[45] R.-J. Slager, L. Rademaker, J. Zaanen, and L. Balents, Phys. Rev. B **92**, 085126 (2015).

[46] L. D. Landau and E. M. Lifshitz, *Electrodynamics of Continuous Media* (Pergamon Press, Oxford, 1960).

[47] L. Ge and L. Feng, Phys. Rev. A **94**, 043836 (2016).

[48] M. Z. Hasan and C. L. Kane, Rev. Mod. Phys. **82**, 3045 (2010).

[49] K. Gottfried and T.-M. Yan, *Quantum Mechanics: Fundamentals*, 2nd ed. (Springer, New York, 2003).

[50] J. D. H. Rivero and L. Ge, Phys. Rev. Lett. **125**, 083902 (2020).

[51] J. D. H. Rivero and L. Ge, Phys. Rev. A **100**, 023819 (2019).

[52] A. Guo, G. J. Salamo, D. Duchesne, R. Morandotti, M. Volatier-Ravat, V. Aimez, G. A. Siviloglou, and D. N. Christodoulides, Phys. Rev. Lett. **103**, 093902 (2009).